Journal of Hazardous Materials 182 (2010) 696–703

Contents lists available at ScienceDirect

Journal of Hazardous Materials

journal homepage: www.elsevier.com/locate/jhazmat

Green, yellow and red emitting CdTe QDs decreased the affinities of apigenin and luteolin for human serum albumin *in vitro*

Jianbo Xiao[a,*], Longsheng Chen[b], Fan Yang[a], Chunxi Liu[a], Yalong Bai[a]

[a] *Institute of Food Engineering, College of Life & Environment Science, Shanghai Normal University, 100 Guilin Rd, Shanghai 200234, PR China*
[b] *Application Research Laboratory, Anhui Academy of Science & Technology, Hefei, Anhui, PR China*

ARTICLE INFO

Article history:
Received 13 April 2010
Received in revised form 31 May 2010
Accepted 19 June 2010
Available online 1 July 2010

Keywords:
QDs size
Apigenin and luteolin
Human serum albumin
Affinity
Fluorescence quenching

ABSTRACT

Apigenin and luteolin were studied for the affinities for human serum albumin (HSA) in the presence and absence of three CdTe QDs with different sizes. The fluorescence intensities of HSA decreased remarkably with increasing concentration of QDs. Apigenin and luteolin resulted in obvious blue-shifts of the λ_{em} of HSA from 340 nm to 330 nm and 320 nm. However, the extents of blue-shifts induced by apigenin or luteolin in the presence of QDs were much smaller than that in the absence of QDs. The quenching process of apigenin for HSA was easily affected by the QDs size than that of luteolin. QDs decreased the quenching constant from 37.23% to 52.38% for apigenin. However, QDs decreased the quenching constant from 56.18% to 60.38% for luteolin. QDs decreased the affinity of apigenin or luteolin for HSA. G-QDs, Y-QDs, and R-QDs decreased the affinity of apigenin for HSA about 14.71%, 12.65% and 6.91%. The binding affinity of apigenin for HSA increased with increasing QDs size. However, the binding affinity of luteolin for HSA decreased with increasing QDs size. G-QDs, Y-QDs, and R-QDs decreased the affinities of luteolin for HSA about 19.48%, 22.47% and 28.18%.

1. Introduction

Dietary flavonoids are the most important polyphenols in plant foods such as fruits, vegetables, nuts, and tea [1,2]. Investigation of flavonoids from dietary sources has attracted great interest for their nutritional and medical effects on human. Most of their bioactivities are likely related to the antioxidant abilities of flavonoids [3,4]. The structural difference of flavones significantly affects their absorption, metabolism, and bioactivities [5,6].

Quantum dots (QDs) are colloidal nanoparticles with unique luminescence characteristics and have been increasingly used in biological area [7]. The investigations of hazardous potential of nanopaticles have attracted great interest for their biological application. The median lethal dose of CdTe was determined to be greater than 2000 mg/kg and the toxicity of CdTe was lower than that of Cd [8]. Intravenous injection of QDs to mice will lead to rapid accumulation in the liver and peripheral regions and it can be cleared via the liver within hours to days [9]. Maysinger and co-workers reported that both uncoated and ZnS-coated QDs can induce the accumulation of lipids [10]. Cho et al. found that it causes functional impairments in live cells to long-term exposure to CdTe QDs [11]. The mechanisms mainly involved in both Cd^{2+} and ROS accompanied by lysosomal enlargement and intracellular redistribution [11].

Among bio-macromolecules, serum albumin is the major soluble protein constituent of circulatory system and has many physiological functions, e.g. it serves as a depot protein and a transport protein for many exogenous compounds. Recently, the toxic interaction with serum albumins was widely reported for their drug nanocarriers application. The exogenous ligands, such as drugs and nanoparticles, can bind to albumins and then be transported in the circulatory system. Liang et al. found that the hydrophobic force and sulfhydryl group play a key role in the interaction between BSA and CdTe QDs [12]. However, Zhao et al. indicated that the hydrogen bonds and van der Waals forces are the main binding forces to stabilize the CdTe QDs–BSA complex [13]. Shao et al. speculated that the interaction of CdTe QDs with BSA was mainly attributed to the electrostatic attraction [14]. Xiao et al. proved that binding of colloidal CdSe/ZnS QDs and HSA is a result of the formation of QDs–HSA complex and electrostatic interactions play a major role in stabilizing the complex [15]. These differences may be caused by the different QD size CdTe. However, very little information is available on whether or not the QDs affect the transportation of drug in blood. And few reports have focused on the effect of QDs size on the interaction between small molecules and plasma proteins. Flavonoid–protein interactions are expected to modulate the bioavailability of flavonoids. The bioactivity of flavonoids is often executed in complex biological systems such as

* Corresponding author. Tel.: +86 136 11600163; fax: +86 021 6432276.
E-mail address: jianboxiao@yahoo.com (J. Xiao).

0304-3894/$ – see front matter © 2010 Elsevier B.V. All rights reserved.
doi:10.1016/j.jhazmat.2010.06.088

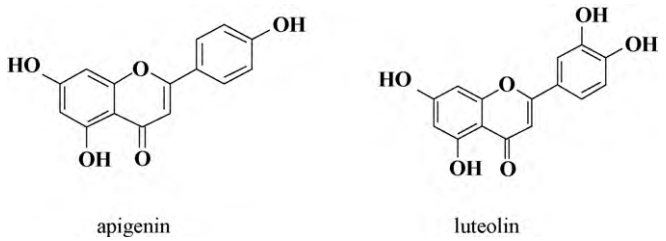

Fig. 1. Structures of apigenin and luteolin.

in blood where various interactions take place. The reversible and irreversible interactions of protein–flavonoid depend on pH, temperature, and concentrations of protein and flavonoid. The binding of small molecules to plasma proteins is a very important parameter for drug metabolism and pharmacokinetic studies. Determining the level of binding of drug for the plasma proteins in the presence and absence of nanoparticles, therefore, is critical and will directly correlate with *in vivo* efficacy of the nanoparticles. Herein, apigenin and luteolin (Fig. 1) were studied for the affinities for human serum albumin (HSA) in the presence and absence of CdTe QDs with different size.

2. Experimental

2.1. Reagents

Apigenin and luteolin (99.0%) were purchased from Tongtian Co. (Shanghai, China) and used without further purification. The working solution of flavones (1.0×10^{-3} mol/L) was prepared by dissolving flavones with methanol. HSA was purchased from Sigma Co. (MO, USA). The working solution of HSA (1.0×10^{-5} mol/L) was prepared with PBS buffer and stored in refrigerator prior to use. 3-Mercaptopropionic acid (MPA, >99%) was provided by Alfa Aesar (Ward Hill, USA). $NaBH_4$ (96%), tellurium powder (99.999%, 200 mesh) and $CdCl_2{\cdot}2.5H_2O$ (99%) were obtained from Shanghai Reagent Co. (Shanghai, China). 1-Ethyl-3-(3-dimethylaminopropyl) carbodiimide hydrochloride (EDC·HCl) and 1-hydroxy-2,5-pyrrolidimedione (NHS) were purchased from Fluka Co. (Buchs, Switzerland). All other reagents and solvents were of analytical reagent grade and used without further purification unless otherwise noted. All aqueous solutions were prepared using newly double-distilled water.

2.2. Apparatus

Fluorescence experiments were performed on a Varian Cray/E spectrofluorophotometer (Palo Alto, USA). UV–vis absorption spectra were carried out on a Varian Cary 50 UV–vis spectrometer (Palo Alto, USA). The transmission electron microscope (TEM) measurement was carried out on a Hitachi H-600 TEM (Tokyo, Japan). Magnetic stirring was carried out using an IKA RH KT/C magnetic stirrer (Staufen, Germany).

2.3. Preparation of NaHTe

NaHTe was used as the Te precursor for CdTe QDs synthesis. It was prepared as described in previous papers [16,17] with slight modifications. Briefly, 31.9 mg of Te powder was mixed with 28.4 mg $NaBH_4$ in a round bottom flask fitted with a rubber stopper. After the flask was filled with N_2, 5 mL of N_2-saturated water was added through a syringe. The reaction was carried out at 25 °C with vigorous magnetic stirring for about 1 h. The reaction was completed when the black Te powder was transformed to white precipitation.

2.4. Synthesis of aqueous-compatible CdTe QDs

Aqueous-compatible CdTe QDs were prepared using the reaction between $CdCl_2{\cdot}2.5H_2O$ and NaHTe solution in the presence of MPA as a stabilizer based on a method reported previously [18,19] with slight modifications. Typically, the freshly prepared NaHTe solution was added to 224 mL of N_2-saturated $CdCl_2{\cdot}2.5H_2O$ solution (2×10^{-2} mol/L) containing 104.4 μL MPA. Then, the solution was adjusted to pH 9.2 with concentrated alkaline and deaerated with nitrogen flow for another 30 min. The typical molar ratio of Cd^{2+}/Te^{2-}/TGA was 1:0.5:2.4. The resulted mixture was heated to 100 °C and refluxed for different times to control the size of CdTe QDs under nitrogen atmosphere.

2.5. Fluorescence spectra

Fluorescence analysis was performed on a Varian Cray/E spectrofluorophotometer in the ratio mode with temperature maintained by circulating bath. The spectra were recorded in the wavelength range of 310–450 nm upon excitation at 295 nm when HSA samples were titrated with QDs or flavonoid. Slit widths (5 nm), scan speed (240 nm/min), and excitation voltage (400 V) were kept constant within each data set and each spectrum was the average of three scans. Quartz cells (1 cm path length) were used for all measurements. Titrations were performed manually by using trace syringes. In each titration, the fluorescence spectrum was collected with the concentrations of HSA at 1.0×10^{-5} mol/L. The experiments were repeated and found to be reproducible within experimental errors.

2.6. Determination of binding parameters

Fluorescence quenching was described by the Stern–Volmer equation [20]:

$$\frac{F_0}{F} = 1 + K_q\tau_0[Q] = 1 + K_{SV}[Q] \quad (1)$$

where F_0 and F represent the fluorescence intensities of fluorophore in the absence and in the presence of quencher, K_q is the quenching rate constant of the bimolecular, K_{SV} is the dynamic quenching constant, τ_0 is the average lifetime of the fluorophore without quencher, and [Q] is the concentration of quencher.

In many instances, the fluorophore can be quenched both by collision and by complex formation with the same quencher. In this case, the Stern–Volmer plot exhibits an upward curvature, concave toward the y-axis at high [Q], and F_0/F is related to [Q] by the modified form of the Stern–Volmer equation [23]:

$$\frac{F_0}{F} = (1 + K_D[Q])(1 + K_S[Q]) \quad (2)$$

where K_D and K_S are the dynamic and static quenching constants, respectively.

The binding constants were calculated according to the double-logarithm equation [20–23]:

$$\frac{\mathrm{Log}_{10}(F_0 - F)}{F} = \mathrm{Log}_{10}K_a + n\mathrm{Log}_{10}[Q] \quad (3)$$

where K_a is the binding constant and n is the number of binding sites per HSA.

3. Results and discussion

3.1. Characterization of CdTe QDs

The CdTe QDs precursor was refluxed with different times to control the nanocrystal size. And then, three different CdTe

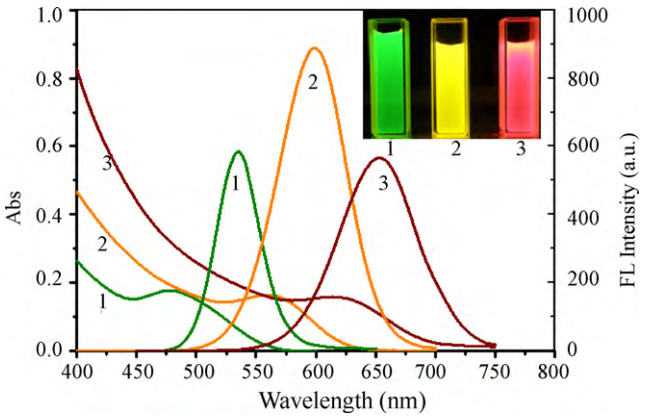

Fig. 2. Absorption spectrum and fluorescence spectrum of CdTe QDs refluxed for different times (1, G-QDs; 2, Y-QDs; 3, R-QDs).

QDs with maximum emissions of 535 nm (green emitting, G-QDs), 598 nm (yellow emitting, Y-QDs), 654 nm (red emitting, R-QDs) were obtained (Fig. 2). The luminescence of all QDs is bright under the UV lamp and the color variation is distinct. Besides fluorescence spectra, the absorption spectra are also shown in Fig. 2. Likewise, with the increasing refluxing time, a large red-shift of the maximum absorption peak took place, and the distinctive peak shape was transformed into smooth shoulder peak gradually. The maximum absorption peaks of G-QDs, Y-QDs, and R-QDs are located at 490 nm, 560 nm, and 614 nm, respectively. According to Peng's empirical formula $D = (9.8127 \times 10^{-7})\lambda^3 - (1.7147 \times 10^{-3})\lambda^2 + 1.0064\lambda - 194.84$ [24], the diameters are 2.04 nm, 3.34 nm, and 3.79 nm, respectively. Furthermore, CdTe QDs were characterized by TEM (Fig. 3). As shown in Fig. 3, the particle size distribution of QDs is relatively uniform.

3.2. Quenching of HSA fluorescence by QDs

HSA has three intrinsic fluorophores: tryptophan, tyrosine and phenylalanine. Because the quantum yield of phenylalanine is very low and the fluorescence of tyrosine is almost totally quenched, the intrinsic fluorescence of HSA is almost entirely due to tryptophan. We measured the fluorescence emission spectra of HSA at a series of concentrations of QDs by fixing the excitation wavelength at 295 nm. The fluorescence emission peak of HSA at 340 nm gives the information of tryptophan residues.

The fluorescence spectra of HSA with addition of QDs were shown in Fig. 4. The fluorescence intensities of HSA decreased remarkably with increasing concentration of QDs. These results suggested that there was a change in the immediate environment of the tryptophan residues and the fact that the flavonoids were situated at close proximity to the tryptophan residues for the quenching to occur. The fluorescence of HSA is primarily from the tryptophan residues. When the excitation wavelength is 295 nm, the fluorescence emission shows the characteristic of tryptophan residues. In the present study, the information about other amino acid residues was not understood. This means that the molecular conformation of the protein was affected, which is in agreement with recent studies that have shown that the tertiary structure of proteins changes upon binding to ligands [20–23]. The buried indole group of Trp could be re-deployed in a more hydrophobic environment after addition of QDs, which agreed to a recent study that has shown that the tertiary structure of proteins changes upon binding of QDs [12], silica-coated CdTe QDs [25], and thiol capped CdTe QDs [26]. When the concentration of QDs approached to 15 μmol/L, the fluorescence intensity of HSA hardly decreased.

The quenching ratios (F/F_0) of HSA fluorescence with addition of G-QDs, Y-GDs and R-QDs were shown in Fig. 5. Approximately 42%, 43% and 55% of the HSA fluorescence were quenched when 15 μmol/L of G-QDs (2.04 nm), R-QDs (3.34 nm), and Y-GDs (3.79 nm) were added, respectively. These results are similar to our previous report that the quenching effect of QDs with different sizes on HSA fluorescence was different from each other [23]. For further discussion, the concentration of QDs was fixed as 15 μM. Fig. 6 showed the Stern–Volmer plots for the HSA fluorescence quenching by QDs. As shown in Fig. 6, the Stern–Volmer plots significantly deviated from linearity toward the *y*-axis at high QDs concentrations, which indicated that both dynamic and static quenching were involved for QDs on HSA fluorescence.

3.3. Quenching of HSA fluorescence by apigenin or luteolin

Upon addition of apigenin and luteolin to the HSA solution, the fluorescence quenching of HSA occurred. The fluorescence intensity attenuated gradually with increasing concentration of apigenin or luteolin. Approximately 75% and 86% of fluorescence quenching was observed when the concentration of apigenin/luteolin reached 10.0 μM (Fig. 7). The extent of the fluorescence attenuation is in the order: apigenin < luteolin, which is just coincidental with the number variation of the substituted hydroxyl on the B-ring of corresponding flavone. The result suggests a key role of the B-ring

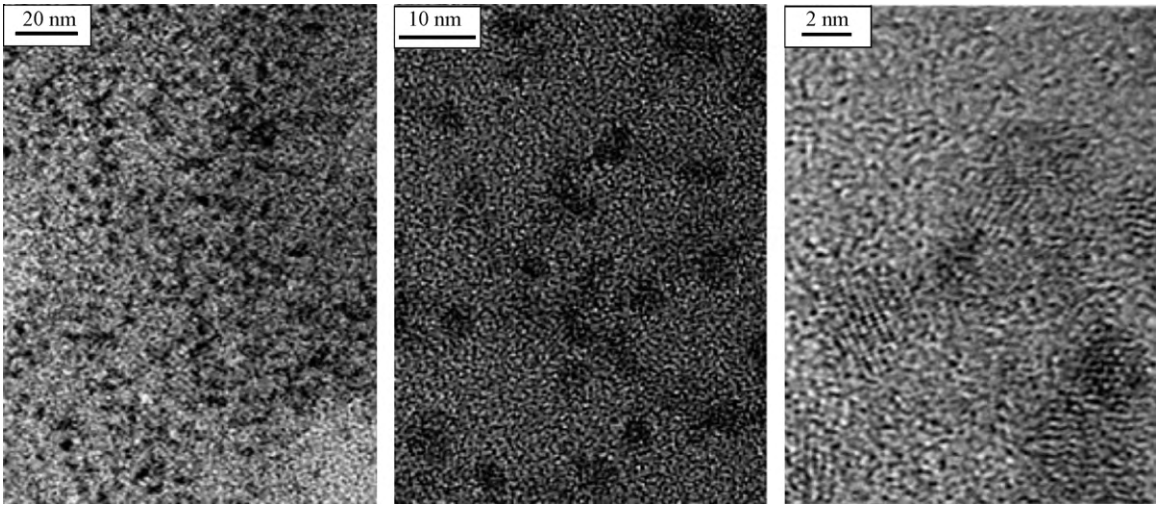

Fig. 3. TEM images of R-QDs. (The scale bars are 20 nm, 10 nm, 2 nm from left to right.)

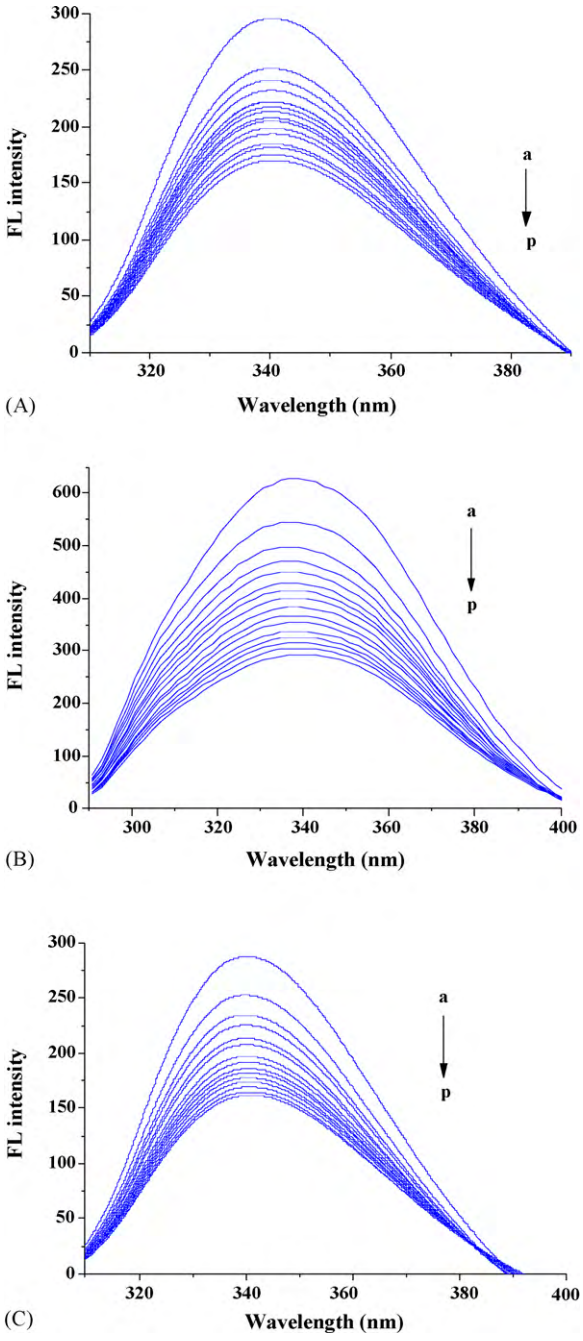

Fig. 4. The quenching effects of QDs on HSA fluorescence intensity. λ_{ex} = 295 nm; HSA, 1.00×10^{-5} mol/L; a–p: 0.00, 1.00, 2.00...15.00 ($\times 10^{-6}$ mol/L) of G-QDs (A), Y-QDs (B), R-QDs (C).

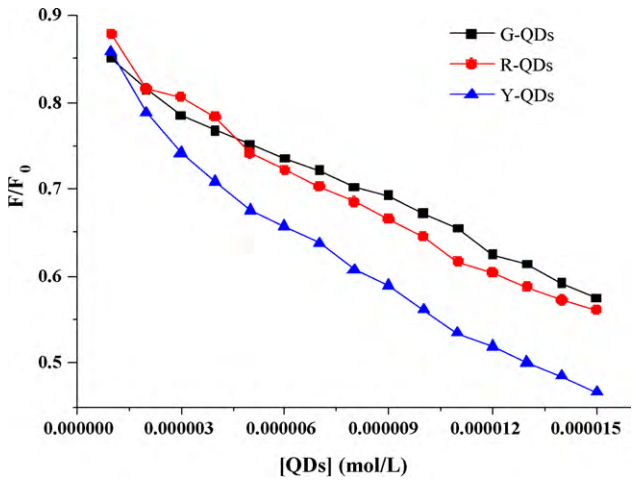

Fig. 5. The quenching ratio (F/F_0) of HSA fluorescence with addition of QDs.

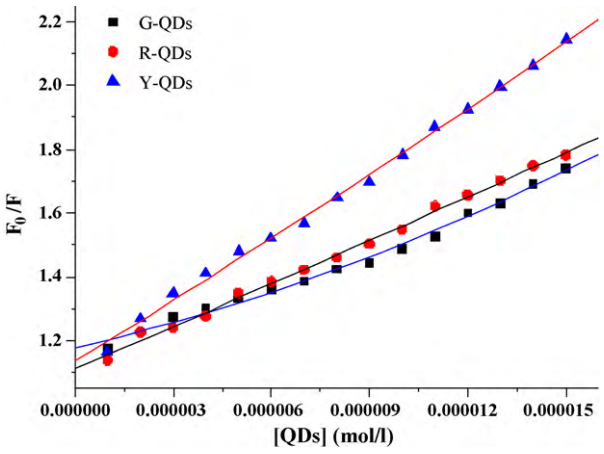

Fig. 6. The Stern–Volmer plots for HSA fluorescence quenching by QDs.

hydroxyl and a distinct effect of its number in the interactions. In addition, apigenin and luteolin resulted in obvious blue-shifts of the maximum emission of HSA from 340 nm to 330 nm and 320 nm, respectively, which is also correlated slightly to the number of B-ring hydroxyl.

The obvious blue-shifts of the maximum λ_{em} of HSA are indicative of changes in the immediate environment of the Trp residues, typically, the polarity of Trp residues and the hydrophobic cavity of HSA. The hydrophobic groups are in the interior of the tertiary structure and the polar groups are on the surface of native protein. The emission of HSA may be blue-shifted if the indole groups of Trp residues are buried within native protein, and its emission may be red-shifted when the protein is unfolded. The result suggests that a greater change in the immediate environment of the Trp residues occurred and flavone was close proximity to or on the surface of the Trp residues. The buried indole group of Trp could be re-deployed in a more hydrophobic environment after addition of flavone. Thus, the molecular conformation of the protein was affected, which agreed to a recent study that has shown that the tertiary structure of proteins changes upon binding of flavones [20–23]. These results indicated that the quenching effect of flavones on HSA fluorescence depended on the structures of flavone. Fig. 8 showed the Stern–Volmer plots for the HSA fluorescence quenching by apigenin and luteolin. In the linear range of Stern–Volmer regression curve the average quenching constants (K_{SV}) for apigenin and luteolin (having the lowest quenching effect, inset in Fig. 8) at 300.15 K were 2.31×10^5 L/mol (R = 0.9995) and 3.81×10^5 L/mol (R = 0.9966), respectively. Because the fluorescence lifetime of the biopolymer is 10^{-8} s [27], the quenching constants K_q for apigenin and luteolin at 300.15 K were calculated to be 2.31×10^{13} L mol^{-1} s^{-1} and 3.81×10^{13} L mol^{-1} s^{-1}, respectively. According to the literatures [20–23], for dynamic quenching, the maximum scatter collision quenching constant of various quenchers with the biopolymer is 2.0×10^{10} L mol^{-1} s^{-1}. Considering that in our experiment the rate constant of the HSA quenching procedure initiated by apigenin and luteolin is much greater than 2.0×10^{10}. According to the literatures [20–23], for dynamic quenching, the maximum scatter collision quenching constant of various quenchers with the biopolymer is 2.0×10^{10} L mol^{-1} s^{-1}; it can be concluded that the nature of quenching is not dynamic

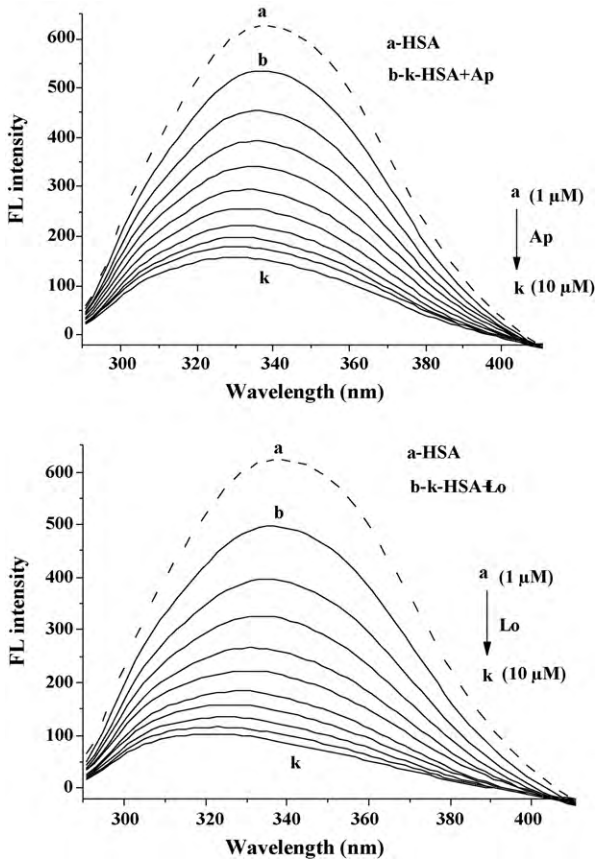

Fig. 7. The quenching effects of apigenin and luteolin on HSA fluorescence intensity. λ_{ex} = 295 nm; HSA, 1.00×10^{-5} mol/L; a–p: 0.00, 1.00, 2.00. . .10.00 ($\times 10^{-6}$ mol/L) of apigenin and luteolin.

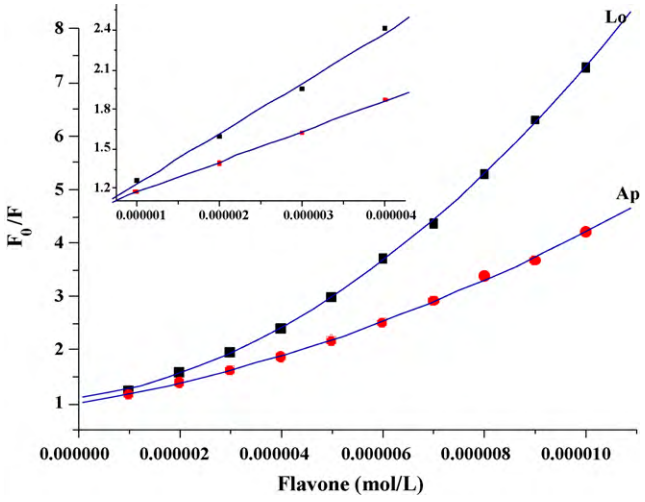

Fig. 8. The Stern–Volmer plots for HSA fluorescence quenching by apigenin and luteolin.

but probably static, resulting from the formation of flavone–HSA complex.

3.4. Fluorescence quenching of HSA induced by apigenin or luteolin in the presence of QDs

When the apigenin or luteolin was continuously added to the HSA solution (1.00×10^{-5} M) containing 15 μM of QDs, further attenuation in the fluorescence of HSA was observed (Fig. 9). When apigenin in the final concentration (8.00 μmol/L) was added, the fluorescence decreased by 71.2%, 69.8%, and 74.6% in the presence of G-QDs, R-QDs, and Y-GDs, respectively, from the original G-QDs-, R-QDs-, and Y-GDs-resulted 42%, 43%, and 55%. When luteolin in the final concentration (8.00 μmol/L) was added, the fluorescence decreased by 73.9%, 70.2%, and 77.2% in the presence of G-QDs, R-QDs, and Y-GDs, respectively, from the original G-QDs-, R-QDs-, and Y-GDs-resulted 42%, 43%, and 55%.

In addition, the obvious blue-shifts of the maximum emission of HSA with the addition of apigenin or luteolin were also observed in the presence of QDs. However, the extents of shifts induced by apigenin or luteolin in the presence of QDs were much smaller than that in the absence of QDs. The λ_{em} of HSA induced by apigenin was changed from 340 nm to 333 nm, 335 nm, and 336 nm in the presence of G-QDs, R-QDs, and Y-GDs, respectively. The λ_{em} of HSA induced by luteolin was changed from 340 nm to 333 nm, 337 nm, and 335 nm in the presence of G-QDs, R-QDs, and Y-GDs, respectively.

Fig. 10 showed the Stern–Volmer plots for the HSA fluorescence quenching by apigenin and luteolin in the presence of QDs. As shown in Fig. 10, the Stern–Volmer plots largely deviated from linearity toward the *y*-axis at high flavone concentrations. Fluorescence quenching could proceed via different mechanisms, usually classified as dynamic quenching and static quenching. According to Soares et al. [28], these deviations indicated there are two distinct situations. In many cases, this upward curvature showed that the fluorophore was quenched by both mechanisms with the same quencher. However, in other cases, the upward curvature illustrated the presence of a sphere of action. Quenching occurs due to the quencher being adjacent to the fluorophore at the moment of excitation. This type of apparent static quenching is usually interpreted in terms of the model "sphere of action" [28].

Table 1 showed the Stern–Volmer quenching constants (K_{SV}) for the interactions of apigenin and luteolin with HSA in the absence and presence of QDs at 300.15 K. As shown in Table 1, the influence of QDs on the quenching constants of apigenin for HSA was determined as follows: R-QDs < G-QDs < Y-QDs. However, the influence of QDs on the quenching constants of luteolin for HSA was determined as follows: Y-QDs < R-QDs < G-QDs. These results indicated that the flavonoid structure and QDs size together affected the binding interaction between flavone and proteins. QDs decreased the quenching constant from 37.23% to 52.38% for apigenin. However, QDs decreased the quenching constant from 56.18% to 60.38% for luteolin. From this point, the quenching process of apigenin for HSA was easily affected by the QDs size than does luteolin.

Table 1
The Stern–Volmer quenching constant K_{SV} for the interactions of apigenin or luteolin with HSA in the absence and presence of QDs at 300.15 K.

	Diameter (nm)	K_{sv} (L/mol)	
		Apigenin	Luteolin
Free	–	2.31×10^5	3.81×10^5
G-QDs	2.04	1.35×10^5	1.51×10^5
Y-QDs	3.34	1.09×10^5	1.67×10^5
R-QDs	3.79	1.47×10^5	1.57×10^5

3.5. Effect of QDs on the affinities of apigenin and luteolin for HSA.

Fig. 11 showed the double-logarithm curves of flavones quenching HSA fluorescence in the presence of QDs at 300.15 K and Table 2 gave the corresponding calculated results. As shown in Table 2, G-QDs, Y-QDs, and R-QDs decreased the affinities of apigenin for HSA about 14.71%, 12.65% and 6.91%. The binding affinity of apigenin for HSA increased with increasing QDs size. However, the binding affinity of luteolin for HSA decreased with increasing QDs size. G-

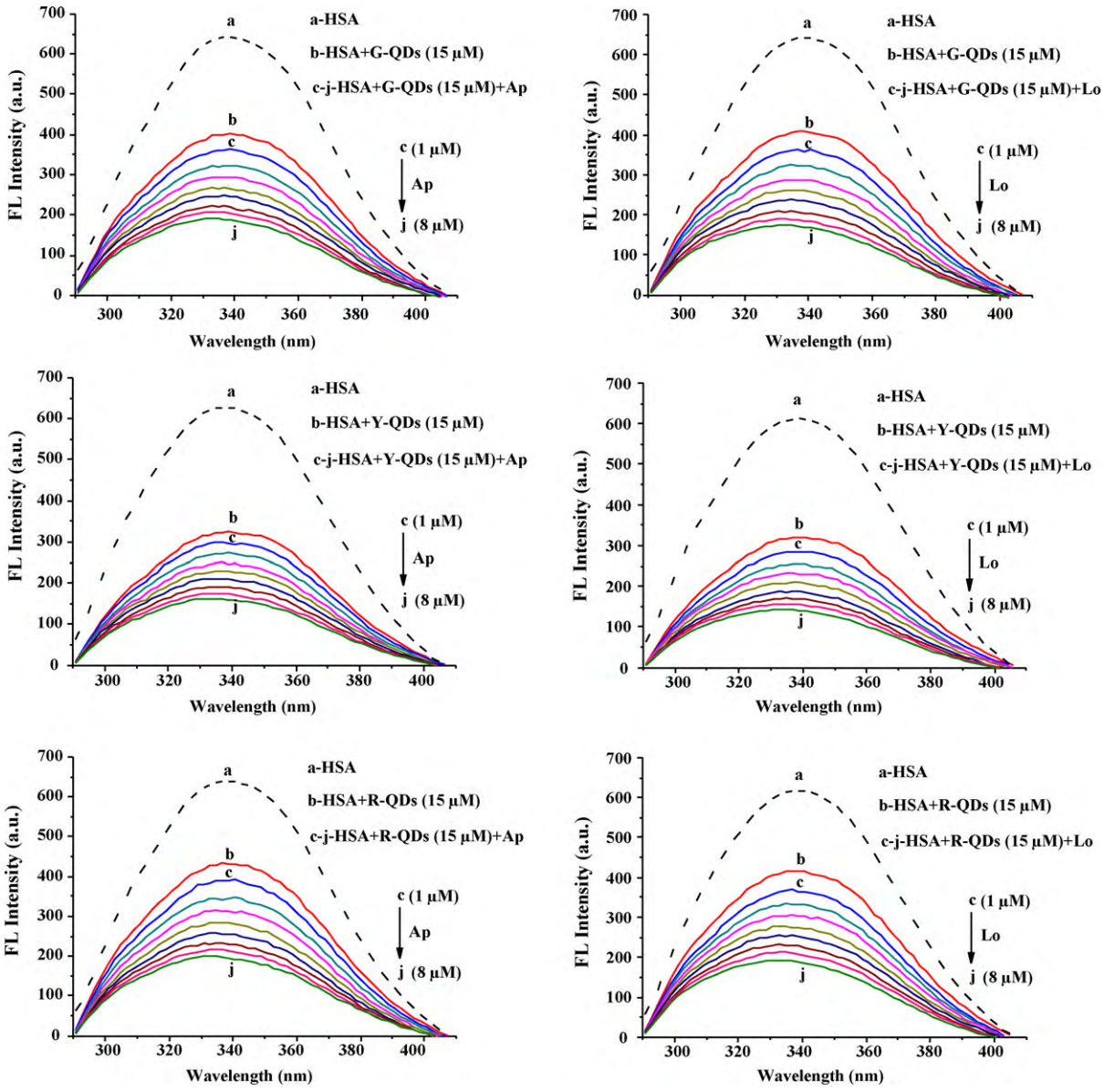

Fig. 9. The fluorescence quenching of HSA by apigenin and luteolin in combination of quantitative QDs (15.00×10^{-6} mol/L). HSA, 1.00×10^{-5} mol/L; flavone (from top to down), 1.00, 2.00, 3.00, 4.00, 5.00, 6.00, 7.00, 8.00 (10^{-6} mol/L); λ_{ex} = 295 nm; T = 300 K.

Table 2
Apparent static binding constants K_a for flavone-HSA in the absence and presence of QDs.

	Apigenin			Luteolin		
	log K_a	n	R	log K_a	n	R
Free	6.80	1.27	0.9983	7.70	1.39	0.9963
G-QDs	5.80	1.13	0.9993	6.20	1.19	0.9991
Y-QDs	5.94	1.17	0.9984	5.97	1.15	0.9993
R-QDs	6.34	1.22	0.9995	5.53	1.07	0.9968

QDs, Y-QDs, and R-QDs decreased the affinities of luteolin for HSA about 19.48%, 22.47% and 28.18%. As shown in Table 2, the hydroxylation on position 3′ of flavone improves the binding affinity for HSA in the absence of QDs. The affinity of luteolin for HSA is about 7.94 times higher than that of apigenin in the absence of QDs. However, the hydroxylation of apigenin on ring B did not obviously affect the affinity for HSA in the presence of QDs. The affinity of luteolin for HSA is about 6.90% higher than that of apigenin in the presence of G-QDs. The affinity of luteolin for HSA is almost the same as that of in the presence of Y-QDs. However, the affinity of luteolin for HSA is about 12.78% higher than that of apigenin in the presence of R-QDs.

Recently, the investigations of hazardous potential of QDs and the toxic interaction with serum albumins have attracted great interest for their drug nanocarriers application [29–31]. Core/shell nanoparticles have been prepared and used as a sustained delivery system for protein [32]. Li et al. found that the erythrocytes treated with nano-TiO_2 were different from those treated with micro-TiO_2 [33]. QDs have numerous potential technological applications but may be hazardous as a result of a variety of interactions with biological systems possibly leading to the harmful effects [29]. However, very little information is available on how these nanoparticles will behave once they find their way into the environment. Uncertainties in the environmental effects associated with exposure to engineered nanomaterials raise key questions about potential risks from such exposures and its effect on health [31].

The degree of binding to albumin may have consequences for the rate of clearance of metabolites and for their delivery to cells and

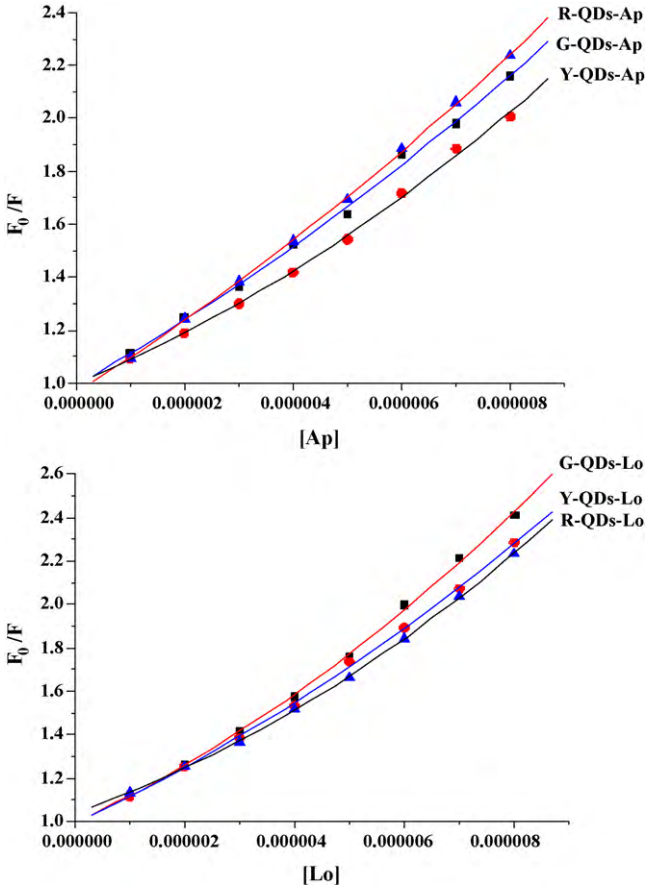

Fig. 10. The Stern–Volmer plots for HSA fluorescence quenching by apigenin and luteolin in the presence of QDs.

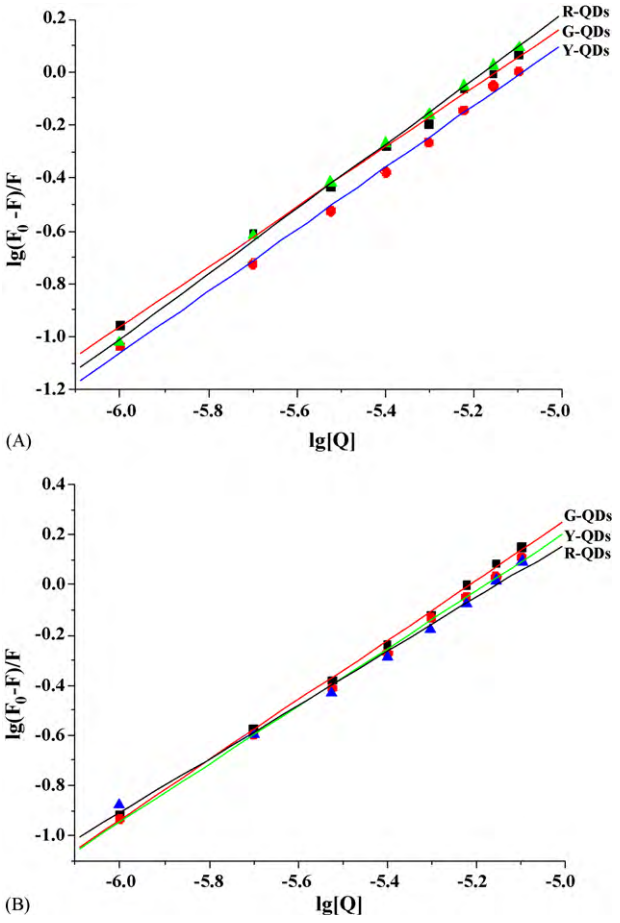

Fig. 11. Double-logarithm curves of apigenin and luteolin quenching HSA fluorescence in the presence of QDs at 300.15 K.

tissues. The conventional view is that the cellular uptake is proportional to the unbound concentration of drugs. According to the free drug hypothesis [34], the flavonoid distribution within the body is generally held to be driven by the free concentration of unbound flavonoid in circulating plasma. The reversible binding to blood proteins, such as serum albumin, α-acid glycoprotein and lipoproteins, may have consequences for the delivery of the flavonoid and their metabolites to cells and tissues. If a molecule is highly bound to plasma proteins, the amount of drug available to diffuse into the target tissue may be significantly reduced and the efficacy of the drug may consequently be poor. Here, it was found that QDs decreased the affinities of apigenin or luteolin for HSA. QDs or nanoparticles in blood will affect the transporting ability of serum albumin for apigenin and luteolin, which may improve the free concentrations of unbound apigenin and luteolin and enhance the pharmacology effects of apigenin and luteolin.

3.6. Relationship between the binding constants (K_a) and the number of binding sites (n)

The obtained values n (1.07–1.39) corresponds to the binding sites with high affinity; however the existence of the low affinity sites was not studied in this work. Recently Berezhkovskiy illustrated that the calculated number of binding sites increased with the increase of compound concentration using the measured values of unbound drug fraction [35]. The number of binding sites (n) is different from the number of molecules actually bound to the sites [35,36]. The number of molecules bound to the binding sites of a bio-macromolecule follows a binomial distribution, if the number of binding sites is fixed [36]. When binding to the receptor with n sites of the same reaction is considered, and $K_d = 1/K_a$ is the dissociation binding constant (affinity of the binding site), it is necessary to have the ligand concentration roughly equal to $10K_d$ to occupy 90% of the binding sites. The low affinity site (K_d about or greater than 1000 μM^{-1}) was not practically occupied (compared to the binding sites with high affinity) and thus was not detected at low concentration of flavones used in the experiments. Though if the number of low affinity sites is significant (for instance 10 with $K_d = 1000\ \mu M^{-1}$), binding to them will be comparable to binding to

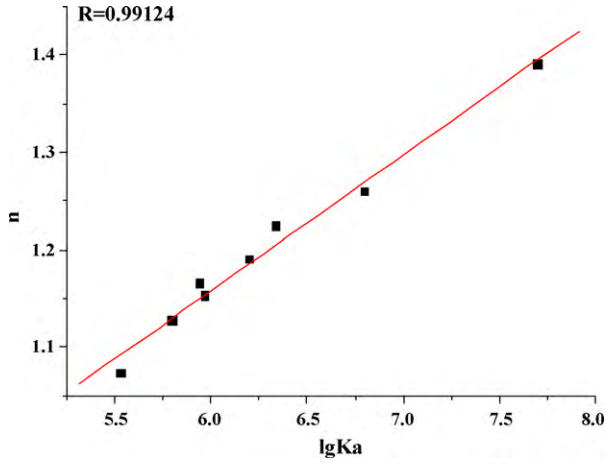

Fig. 12. The relationship between the affinities ($\log_{10} K_a$) and the number of binding sites (n) between flavones and HSA.

a single high affinity site. This is because the increase of the quantity of sites leads to the increase of ligand bound to them. So the number of binding sites increasing with increasing binding constant can be considered as one theory to evaluate these models. The relationship between the $\log_{10}(K_a)$ and the number of binding sites (n) between flavones and serum albumins was shown in Fig. 12. The values of $\log_{10} K_a$ are proportional to the number of binding sites (n). This result confirms the Eq. (3) used here is suitable to study the interaction between flavones and HSA.

Acknowledgments

The authors are grateful for financial sponsored by Natural Science Foundation of Shanghai (10ZR1421700), "Chen Guang" project supported by Shanghai Municipal Education Commission and Shanghai Education Development Foundation (09CG46), Innovation Program of Shanghai Municipal Education Commission (10YZ68) and Program of Shanghai Normal University (SK201006). The authors also thank Dr. Xinlin Wei and Dr. Yuanfeng Wang for preparing QDs.

References

[1] D. Ghosh, A. Scheepens, Vascular action of polyphenols, Mol. Nutr. Food Res. 53 (2009) 322–331.
[2] E. Sepehr, G.M. Cooke, P. Robertson, G.S. Gilani, Effect of glycosidation of isoflavones on their bioavailability and pharmacokinetics in aged male rats, Mol. Nutr. Food Res. 53 (2009) S16–S26.
[3] L. Pérez-Fons, M.T. Garzón, V. Micol, Relationship between the antioxidant capacity and effect of Rosemary (*Rosmarinus officinalis* L.) polyphenols on membrane phospholipid order, J. Agric. Food Chem. 58 (2010) 161–171.
[4] N. Krafczyk, F. Woyand, M.A. Glomb, Structure-antioxidant relationship of flavonoids from fermented rooibos, Mol. Nutr. Food Res. 53 (2009) 635–642.
[5] K.L. Wolfe, R.H. Liu, Structure–activity relationships of flavonoids in the cellular antioxidant activity assay, J. Agric. Food Chem. 56 (2008) 8404–8411.
[6] X. Wen, T. Walle, Methylated flavonoids have greatly improved intestinal absorption and metabolic stability, Drug Metab. Dispos. 34 (2006) 1786–1792.
[7] A. Wolcott, D. Gerion, M. Visconte, J. Sun, A. Schwartzberg, S. Chen, J.Z. Zhang, Silica-coated CdTe quantum dots functionalized with thiols for bioconjugation to IgG proteins, J. Phys. Chem. B 110 (2006) 5779–5789.
[8] J. Zayed, S. Philippe, Acute oral and inhalation toxicities in rats with cadmium telluride, Int. J. Toxicol. 28 (2009) 259–265.
[9] A. Zintchenko, A.S. Susha, M. Concia, J. Feldmann, E. Wagner, A.L. Rogach, M. Ogris, Drug nanocarriers labeled with near-infrared emitting quantum dots (quantoplexes): imaging fast dynamics of distribution in living animals, Mol. Ther. 17 (2009) 1849–1856.
[10] E. Przybytkowski, M. Behrendt, D. Dubois, D. Maysinger, Nanoparticles can induce changes in the intracellular metabolism of lipids without compromising cellular viability, FEBS J. 276 (2009) 6204–6217.
[11] S.J. Cho, D. Maysinger, M. Jain, B. Röder, S. Hackbarth, F.M. Winnik, Long-term exposure to CdTe quantum dots causes functional impairments in live cells, Langmuir 23 (2007) 1974–1980.
[12] J.G. Liang, Y.P. Cheng, H.Y. Han, Study on the interaction between bovine serum albumin and CdTe quantum dots with spectroscopic techniques, J. Mol. Struct. 892 (2008) 116–120.
[13] L.Z. Zhao, R.T. Liu, X.C. Zhao, B.J. Yang, C.Z. Gao, X.P. Hao, Y.Z. Wu, New strategy for the evaluation of CdTe quantum dot toxicity targeted to bovine serum albumin, Sci. Total Environ. 407 (2009) 5019–5023.
[14] L.W. Shao, C.Q. Dong, F.M. Sang, H.F. Qian, J.C. Ren, Studies on interaction of CdTe quantum dots with bovine serum albumin using fluorescence correlation spectroscopy, J. Fluoresc. 19 (2009) 151–157.
[15] Q. Xiao, S. Huang, Z.D. Qi, B. Zhou, Z.K. He, Y. Liu, Conformation, thermodynamics and stoichiometry of HSA adsorbed to colloidal CdSe–ZnS quantum dots, BBA-Proteins Proteom. 1784 (2008) 1020–1027.
[16] W.H. Yang, W.W. Li, K. Sun, Hydrothermal synthesis of cysteamine-stabilized CdTe quantum dots, Chem. J. Chin. U 29 (2008) 681–685.
[17] Y. Kuo, Q. Wang, C. Ruengruglikit, Q. Huang, Antibody-conjugated CdTe quantum dots for *E. coli* detection, J. Phys. Chem. C 112 (2008) 4818–4824.
[18] Z. Lin, X. Su, H. Zhang, Studies on quantum dots synthesized in aqueous solution for biological labeling, Chem. J. Chin. U. 24 (2003) 216–220.
[19] J. Weng, X. Song, L. Li, H. Qian, K. Chen, X. Xu, C. Cao, J. Ren, Highly luminescent CdTe quantum dots prepared in aqueous phase as an alternative fluorescent probe for cell imaging, Talanta 70 (2006) 397–402.
[20] J. Xiao, X. Chen, L. Zhang, S.G. Talbot, G.C. Li, M. Xu, Investigation the mechanism of enhanced effect of EGCG on huperzine A inhibiting acetylcholinesterase activity in rats by multispectroscopic method, J. Agric. Food Chem. 56 (2008) 910–915.
[21] J.B. Xiao, H. Cao, Y.F. Wang, J.Y. Zhao, X.L. Wei, Glycosylation of dietary flavonoids decreases the affinities for plasma protein, J. Agric. Food Chem. 57 (2009) 6642–6648.
[22] J.B. Xiao, M. Suzuki, X.Y. Jiang, X.Q. Chen, K. Yamamoto, M. Xu, Influence of B-ring hydroxylation on interactions of flavonols with bovine serum albumin, J. Agric. Food Chem. 56 (2008) 2350–2356.
[23] J.B. Xiao, Y.L. Bai, Y.F. Wang, J.W. Chen, X.L. Wei, Systematic investigation of the influence of CdTe QDs size on the toxic interaction with human serum albumin by fluorescence quenching method, Spectrochim. Acta A 76 (2010) 93–97.
[24] W.W. Yu, L.H. Qu, W.Z. Guo, X.G. Peng, Experimental determination of the extinction coefficient of CdTe, CdSe, and CdS nanocrystals, Chem. Mater. 15 (2003) 2854–2860.
[25] A. Wolcott, D. Gerion, M. Visconte, J. Sun, A. Schwartzberg, S. Chen, J.Z. Zhang, Silica coated CdTe quantum dots functionalized with thiols for bioconjugation to IgG proteins, J. Phys. Chem. B 110 (2006) 5779–5789.
[26] M. Idowu, E. Lamprecht, T. Nyokong, Interaction of water soluble thiol capped CdTe quantum dots and bovine serum albumin (BSA), J. Photochem. Photobiol. A 198 (2008) 7–12.
[27] J.R. Lakowicz, Principles of fluorescence spectroscopy, third ed., Springer Science+Business Media, LLC, 233 Spring Street, New York, USA, 2006.
[28] S. Soares, N. Mateus, V. Freitas, Interaction of different polyphenols with bovine serum albumin (BSA) and human salivary R-amylase (HSA) by fluorescence quenching, J. Agric. Food Chem. 55 (2007) 6726–6735.
[29] J. Valanta, D. Drobne, K. Sepčić, A. Jemec, K. Kogej, R. Kostanjšek, Hazardous potential of manufactured nanoparticles identified by *in vivo* assay, J. Hazard. Mater. 171 (2009) 160–165.
[30] A.L. Di Virgilio, M. Reigosa, P.M. Arnal, M.F.L. de Mele, Comparative study of the cytotoxic and genotoxic effects of titanium oxide and aluminium oxide nanoparticles in Chinese hamster ovary (CHO-K1) cells, J. Hazard. Mater. 177 (2010) 711–718.
[31] V. Shah, P. Dobiášová, P. Baldrian, F. Nerud, A. Kumar, S. Seal, Influence of iron and copper nanoparticle powder on the production of lignocellulose degrading enzymes in the fungus Trametes versicolor, J. Hazard. Mater. 178 (2010) 1141–1145.
[32] K.S. Oh, S.K. Han, H.S. Lee, H.M. Koo, R.S. Kim, K.E. Lee, S.S. Han, S.H. Cho, S.H. Yuk, Core/shell nanoparticles with lecithin lipid cores for protein delivery, Biomacromolecules 7 (2006) 2362–2367.
[33] S.Q. Li, R.R. Zhu, H. Zhu, M. Xue, X.Y. Sun, S.D. Yao, S.L. Wang, Nanotoxicity of TiO_2 nanoparticles to erythrocyte *in vitro*, Food Chem. Toxicol. 46 (2008) 3626–3631.
[34] I. Buxton, Pharmacokinetics and pharmacodynamics: the dynamics of drug absorption, distribution, action and elimination, in: L. Brunton (Ed.), Goodman & Gilman's The Pharmacological Basis of Therapeutics, McGraw-Hill, Chicago, 2005, pp. 1–39.
[35] L.M. Berezhkovskiy, On the calculation of the concentration dependence of drug binding to plasma proteins with multiple binding sites of different affinities: determination of the possible variation of the unbound drug fraction and calculation of the number of binding sites of the protein, J. Pharm. Sci. 96 (2007) 249–257.
[36] J.B. Xiao, X.Q. Chen, X.Y. Jiang, M. Hilczer, M. Tachiya, Probing the interaction of transresveratrol with bovine serum albumin: a fluorescence quenching study with Tachiya model, J. Fluoresc. 18 (2008) 671–678.